JMEPEG
https://doi.org/10.1007/s11665-026-14076-7

1059-9495/$19.00

ORIGINAL RESEARCH ARTICLE

Electrodeposition of CoCrFeNiAl High-Entropy Alloy Coatings: Effect of the Deposition Time on the Corrosion Resistance

Fernanda Santos Fogassa, Marina Fuser Pillis, Carlos Triveño Ríos, Renato Altobelli Antunes, and Mara Cristina Lopes de Oliveira

Submitted: 10 October 2025 / Revised: 22 January 2026 / Accepted: 24 April 2026

In this work, CoCrFeNiAl high-entropy alloy coatings were obtained by electrodeposition in aqueous solution, using 1020 carbon steel plates as substrates. The effect of the deposition time on corrosion resistance of the coated samples was evaluated. Four deposition times were tested, 15, 20, 25, and 30 min. The corrosion behavior was studied in 3.5 wt.% NaCl solution, using electrochemical impedance spectroscopy and potentiodynamic polarization tests. The corrosion protection ability was dependent on the plating time. The coated samples exhibited passive corrosion behavior, while the uncoated steel substrate was in an active state. The stability of the passive film was higher at the deposition times of 15 min and 20 min. The passive range for the specimens obtained at a deposition time of 15 min was 3.7 times wider than at 30 min. The improved passive film stability at 15 min deposition was due to the coating morphology. Longer immersion times were detrimental to the protection efficiency, as the coating layer became more defective.

Keywords coatings, CoCrFeNiAl, corrosion, electrodeposition

1. Introduction

Bulk high-entropy alloys (HEAs) are commonly produced by casting methods such as arc induction melting (Ref 1, 2). Mechanical alloying (Ref 3) and rapid solidification (Ref 4) are also employed with the same purpose. Due to the relatively high fraction of expensive metals in many HEA systems, deposition techniques are an attractive technological route to obtain HEA coatings on conventional metallic materials, such as steels. This is an economical way of taking advantage of the superior surface properties imparted by HEAs, while avoiding the high costs of using bulk alloys consisting of many expensive elements (Ref 5, 6). Several deposition techniques have been reported in the literature, such as thermal spraying (Ref 7), laser cladding (Ref 8, 9), magnetron sputtering (Ref 10), and electrodeposition (Ref 11). Particular attention has been paid to electrodeposition of HEAs due to a set of attributes such as the possibility of conducting the deposition process at room temperature, simple experimental configuration, and full control of process parameters, such as potential, current density, and time that allows to tailoring several coating characteristics (morphology, grain size, and composition) (Ref 12, 13). For example, Freitas et al. (Ref 11) developed CoFeNiMoW high-entropy alloy coatings by direct electrodeposition from aqueous solutions. The composition of the deposited coatings was properly controlled by adjusting the current density during galvanostatic electrodeposition. Yoosefan et al. (Ref 14) observed that the corrosion resistance of electrodeposited CoCrFeMnNi coatings deposited on copper substrates was affected by the processing potential.

The interest in the CoCrFeNi HEA system relies on suitable mechanical properties at room temperature and good corrosion resistance (Ref 15, 16). The overall properties of this fundamental HEA system can be enhanced further by incorporating a fifth element, such as Al, Cu, Mn, Ti, Mo, and V, with numerous possible new compositions (Ref 17-21). Addition of Al to the CoCrFeNi HEA system has been shown to affect either the mechanical behavior or electrochemical response (Ref 22). For example, the formation of a thicker passive film for AlCoCrFeNi HEA when compared to CoCrFeNi has been reported by Nascimento et al. (Ref 23), influencing the corrosion resistance of the bulk alloy. Lyu et al. (Ref 24) reported a deleterious effect of Al addition on the corrosion resistance of CoCrFeNiAlx (x = 0.1, 0.05, 1) in sodium chloride solution.

While the correlation between the corrosion behavior and the chemical composition of CoCrFeNiAl bulk HEAs has received much attention in the literature, research is still scarce for electrodeposited coatings. The effect of processing parameters on the corrosion behavior and its correlation with coating microstructure and chemical composition are not well understood yet. Few studies have explored the influence of deposition time on the corrosion resistance of electrodeposited HEA coatings, particularly for the CoCrFeNiAl system.

In the light of this scenario, the aim of the present work was to obtain CoCrFeNiAl HEA coatings on SAE 1020 carbon steel

Fernanda Santos Fogassa, Carlos Triveño Ríos, Renato Altobelli Antunes, and **Mara Cristina Lopes de Oliveira**, Center for Engineering, Modeling and Applied Social Sciences, Federal University of the ABC, Av. Dos Estados, 5001, Santo André, SP 09280-560, Brazil; and **Marina Fuser Pillis**, Instituto de Pesquisas Energéticas e Nucleares Centro de Ciência e Tecnologia de Materiais (CECTM), Av. Prof. Lineu Prestes, 2242, São Paulo, SP 05508-000, Brazil. Contact e-mail: renato.antunes@ufabc.edu.br.

Published online: 08 May 2026

substrates by electrodeposition in aqueous solutions. Furthermore, the effect of the deposition time on the microstructure, chemical composition, and corrosion behavior of the HEA coatings was investigated. X-ray photoelectron spectroscopy (XPS) was used to examine the surface chemical states of the coatings. The microstructure was analyzed by scanning electron microscopy (SEM). The corrosion behavior was assessed by electrochemical impedance spectroscopy and potentiodynamic polarization.

2. Experimental Section

2.1 Material and Sample Preparation

The metallic substrates were SAE 1020 carbon steel plates with approximate dimensions of 30 × 20 × 1 mm. The surface finishing procedure consisted of mechanical grinding with waterproof silicon carbide papers up to grit 1000. Next, the specimens were rinsed with distilled water and naturally dried in open air.

2.2 Electrodeposition

Before deposition, the specimens were degreased with acetone, activated in HCl bath for 10 s, washed with distilled water, and directly placed in the electrolytic glass cell as a cathode. Electrodeposition was conducted in a direct current mode, using a DC power supply (MP5003D, Shenzhen, China) at a constant current density of 50 mA.cm^{-2}, at 35 °C, and without stirring. The anode was a platinum sheet with rectangular dimensions of 4 × 2 cm and thickness of 0.1 cm. The electrodeposition process is illustrated in Fig. 1.

The composition of the deposition bath is shown in Table 1. Chloride salts were used due to their high cathodic efficiency (Ref 25). The process was carried out at 35 °C under magnetic stirring. Several additives were used to enhance surface morphology (ascorbic acid, sulfanilic acid, formic acid, boric acid, and ammonium chloride). All chemicals were reagent grade. The pH was adjusted to 1.5 controlled with NaOH. Four different deposition times were tested: 15, 20, 25, and 30 min. Table 2 shows the sample code employed throughout the text. After electrodeposition, the specimens were rinsed with distilled water and dried with a warm air stream provided by a heat gun.

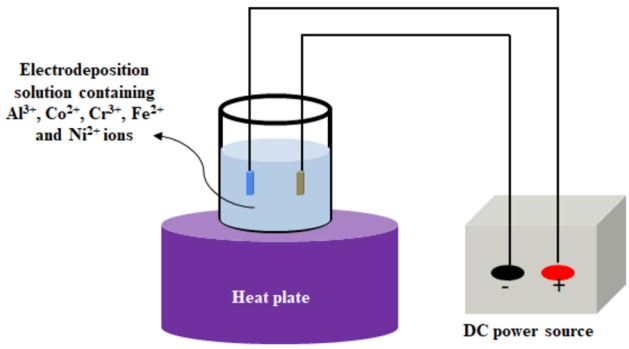

Fig. 1 Illustration of the electrodeposition treatment setup

2.3 Characterization of the HEA Coatings

The surface morphology of the HEA coatings was examined using scanning electron microscopy (Jeol, SEM JSM-IT700HR) equipped with field emission gun (FEG). Cross-sectional images were also acquired for measuring the coating thickness using a FEG-SEM Phenom Pharos G2 (ThermoFisher Scientific). Phase composition was assessed by x-ray diffractometry (Bruker, D8 Discover), using Cu-Kα radiation (λ = 0.154 nm) with θ-2θ configuration in the range of 30-90°.

The surface chemical states of the different elements on the surface of the electrodeposited samples were assessed by x-ray photoelectron spectroscopy (XPS) using a ThermoFisher Scientific spectrometer, model K-alpha^{+} operating with Al-Kα radiation source (1486.6 eV). The spot size was 400 μm. The pressure in the analysis chamber was approximately 10^{-7} Pa. Survey and narrow scan spectra were acquired with pass energies of 200 eV and 50 eV, respectively. The narrow scan spectra were deconvoluted with a mixture of Lorentzian–Gaussian functions in the Avantage© software. The Smart© algorithm was used for background subtraction.

2.4 Electrochemical Tests

The electrochemical tests were carried out with a conventional three-electrode cell configuration with the HEA-coated specimens as the working electrode, a platinum wire as the counter-electrode, and Ag/AgCl (KCl, 3 M) as the reference electrode. To evaluate the general corrosion behavior of the samples, the tests were conducted in a 3.5 wt.% NaCl solution at room temperature. Initially, the open-circuit potential (OCP) was monitored for 1 h. Next, electrochemical impedance spectroscopy (EIS) measurements were performed at the OCP in the frequency range of 100 kHz-10 mHz with an amplitude of the sinusoidal perturbation signal of ± 10 mV (rms) and acquisition of 10 points per frequency decade. Following EIS, the specimens were subjected to potentiodynamic polarization at a scanning rate of 1 mV.s^{-1} between − 0.3 and + 1.0 V versus the OCP. All tests were carried out in an Autolab M101 potentiostat/galvanostat. The tests were conducted in triplicate.

3. Results

3.1 Structural Characterization

Figure 2 shows the XRD patterns of the CoCrFeNiAl samples. The diffraction peaks are broad and exhibited low intensity, revealing an amorphous character that was also reported for other electrodeposited FeCoNi-HEA systems (Ref 26). As the deposition time increased, the peaks became more intense and narrower, suggesting the formation of a body-centered cubic (BCC) nanocrystalline solid solution in accordance with the results published by Wang et al. (Ref 27), who identified one single BCC structure for AlxCoCrFeNi high-entropy alloys.

3.2 Morphological Aspects and Coating Composition

Figure 3 shows the top-surface SEM micrographs of the CoCrFeNiAl HEA electrodeposited coatings obtained at different deposition times. The barrier properties of electrodeposited coatings depend on their compactness which, in turn, is affected by the deposition time (Ref 28). The HEA-15 layer

Table 1 Bath composition and operating conditions for obtaining the CoCrFeNiAl HEA electrodeposited coatings

CoCrFeNiAl HEA coating		
Electrolyte composition	**Concentration, g.L^{-1}**	**Operating condition**
$CrCl_3.4H_2O$	37	pH 1.5
$CoCl_2.6H_2O$	9	Temperature 35 °C
$FeCl_2.4H_2O$	8	Magnetic stirring
$NiCl_2.6H_2O$	17	Current density 50 mA.cm^{-2}
$AlCl_3.6H_2O$	24	

Table 2 Sample code used throughout the text

HEA coating	Sample code	Deposition time, min
CoCrFeNiAl	HEA-15	15
	HEA-20	20
	HEA-25	25
	HEA-30	30

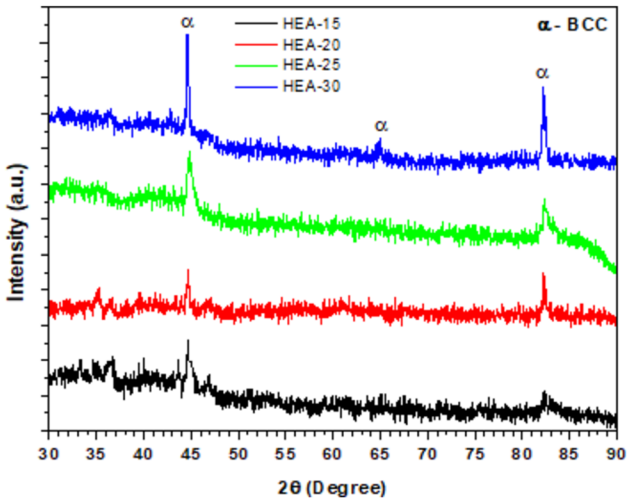

Fig. 2 XRD patterns of the CoCrFeNiAl HEA electrodeposited coatings obtained at different deposition times

(Fig. 3a) exhibited compact surface morphology. Figure 3(b) shows that HEA-20 coating exhibited a granular topography with several microcracks spread over the surface. HEA-25 (Fig. 3c) is characterized by an irregular surface, with several microcracks, as shown inside the circled area. HEA-30 topography was clearly dominated by cracked regions over the whole surface (Fig. 3d).

The cross-sectional SEM micrographs of the HEA coatings are shown in Fig. 4. The HEA-15 sample exhibited a homogeneous distribution over the examined area, as indicated in Fig. 4(a). For longer deposition times, the coating thickness increased, as observed in Fig. 4(b), (c) and (d). However, the increased thickness was accompanied by the growth of defective layers, heterogeneously distributed at the interface with the substrate.

3.3 XPS Analysis

Representative XPS narrow scan spectra obtained for the HEA-15 sample are shown in Fig. 5. The spectrum for the Co $2p_{3/2}$ photoelectron lines (Fig. 5a) was deconvoluted with three peaks. The metallic component (Co_{met}) is centered at 778.7 eV. The Co^{2+} and Co^{3+} oxidized states appear at higher binding energies, indicating the presence of CoO and Co_3O_4, as reported by other authors (Ref 29, 30). The Cr $2p_{3/2}$ spectrum (Fig. 5b) exhibited the presence of Cr^{3+} species (Cr_2O_3 and $Cr(OH)_3$), while metallic chromium, which appears at approximately 574 eV (Ref 31), was not found. The Fe $2p_{3/2}$ spectrum (Fig. 5c) was fitted with a five-peak set which was attributed to metallic iron (Fe_{met}), Fe_3O_4, FeO, Fe_2O_3, and FeOOH, showing a mixture of Fe^{2+} and Fe^{3+} species, in good agreement with the literature (Ref 32, 33). The Ni $2p_{3/2}$ spectrum (Fig. 5d) was fitted with three peaks referred to metallic nickel (Ni_{met}), NiO, and $Ni(OH)_2$ with predominance of the metallic state. The relatively low oxidation susceptibility of Ni when compared to Fe and Cr (Ref 34) is likely related to the predominance of Ni_{met}. The surface chemical states of Al are shown in the Al 2p spectrum (Fig. 5e). Only Al^{3+} species were found, Al_2O_3 and Al(OOH), and the peak of metallic Al, which is centered at approximately 72 eV, was absent. Peak positions are in good agreement with the literature (Ref 35, 36). The O 1 s spectrum is shown in Fig. 5(f). The spectrum was fitted with three components which were assigned to oxide (O^{2-}) and hydroxide (OH^-) bonds, along with adsorbed water (H_2O_{ads}) at approximately 533 eV, as reported by other authors (Ref 37, 38).

3.4 Corrosion Behavior

Figure 6 shows the potential versus time curves for the HEA samples. The uncoated substrate is included for comparison. The tests were carried out in 3.5 wt.% NaCl solution at room temperature. All samples exhibited nobler potential values than the uncoated carbon steel substrate, indicating the reduced electrochemical activity of the HEA film with respect to the pristine surface. The potential was shifted to more anodic values for the HEA-15 sample when compared to the other HEA-coated samples. The potential shift toward nobler values is often regarded as an indication of lower corrosion susceptibility, being associated with a stable surface (Ref 39).

Figure 7 shows the EIS test results of the uncoated and HEA-coated 1020 carbon steel samples after 1 h of immersion in 3.5 wt.% NaCl at room temperature. To ensure that the EIS results were valid based on the constraints of the linear system theory (LST), we checked the causality, linearity, and stability of the systems using Kramers–Kronig (K-K) transforms in the Nova 2.1.7 software. The K-K transforms are plotted as solid lines, superimposed to the experimental data in Fig. 7. This is a

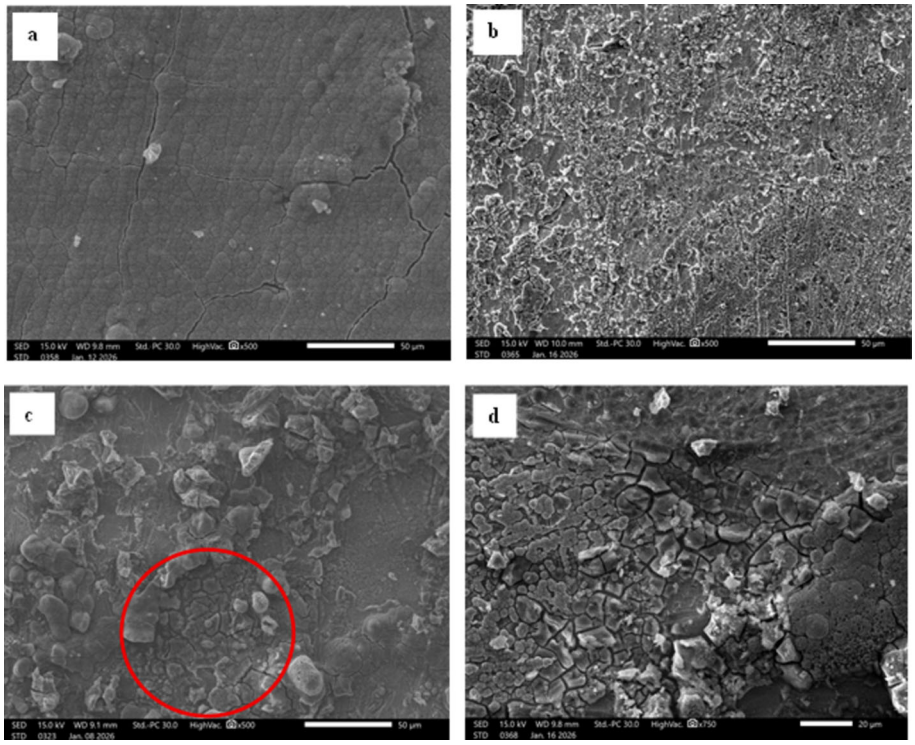

Fig. 3 SEM micrographs (top surfaces) of the CoCrFeNiAl HEA electrodeposited coatings obtained at different deposition times: (a) HEA-15; (b) HEA-20; (c) HEA-25; and (d) HEA-30

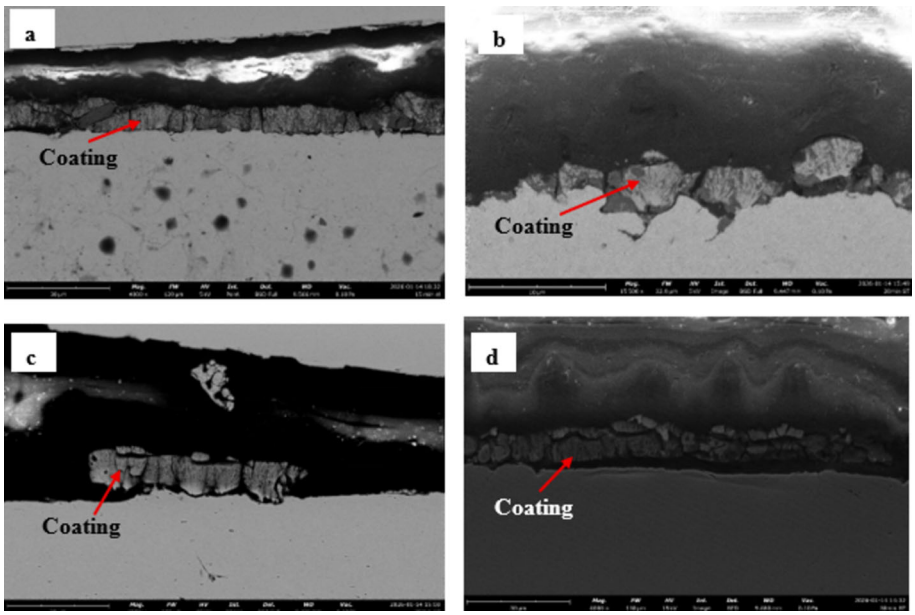

Fig. 4 SEM micrographs (cross sections) of the CoCrFeNiAl HEA electrodeposited coatings obtained at different deposition times: (a) HEA-15; (b) HEA-20; (c) HEA-25; and (d) HEA-30

well-accepted method of evaluating the validity of EIS measurements (Ref 40, 41). As shown in Fig. 7, there is a good match between the K-K transforms and their corresponding experimental data for all samples. The quality of the fitting results was assessed by the χ^2 parameter. All coated samples exhibited values as low as 10^{-6}, revealing a remarkable coincidence between K-K transforms and the measured data.

The Nyquist plots (Fig. 7a) of the uncoated substrate are characterized by a capacitive loop in the high- to middle-frequency range, with an inductive response in the low-frequency domain. This behavior is typical of bare carbon steel substrates in chloride-containing solutions, being associated with the adsorption/desorption of Cl^- during charge transfer reactions at metal/electrolyte interface of the unprotected metallic surface (Ref 42). The inductive loop was not observed

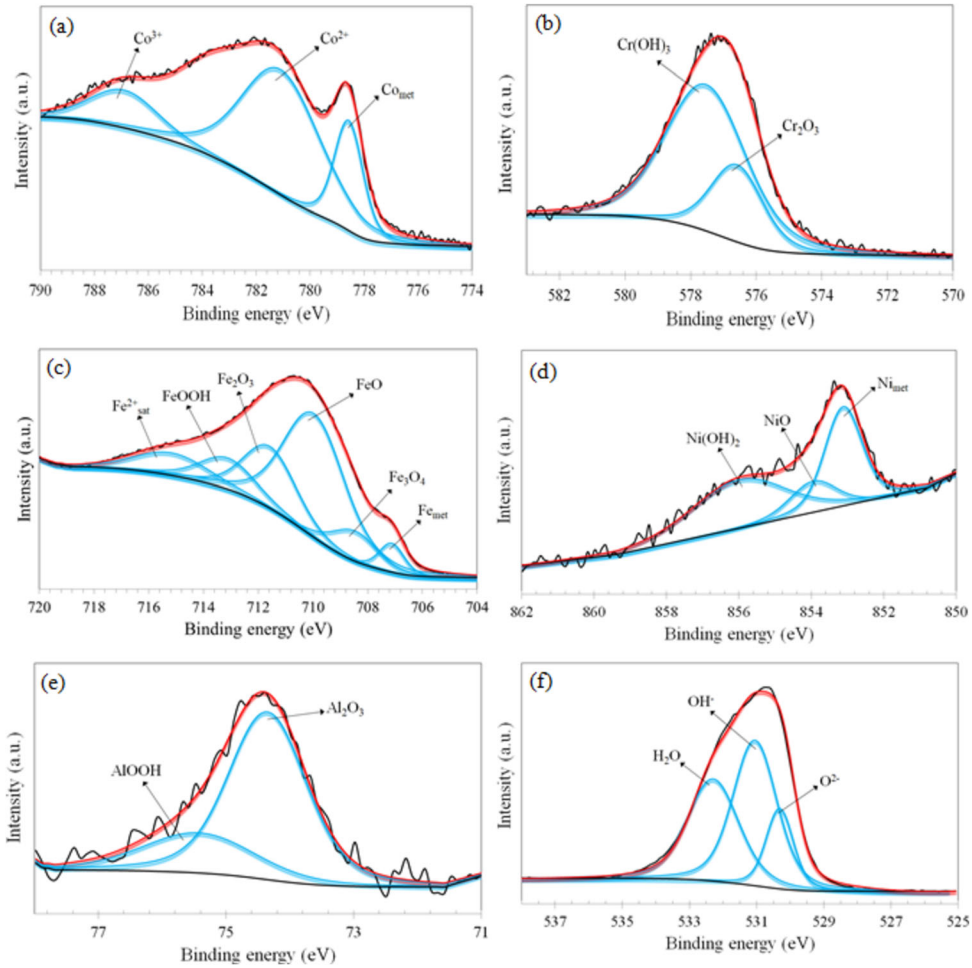

Fig. 5 XPS narrow scan spectra of the HEA-15 sample: (a) Co $2p_{3/2}$; (b) Cr $2p_{3/2}$; (c) Fe $2p_{3/2}$; (d) Ni 2p; (e) Al 2p; and (f) O 1 s

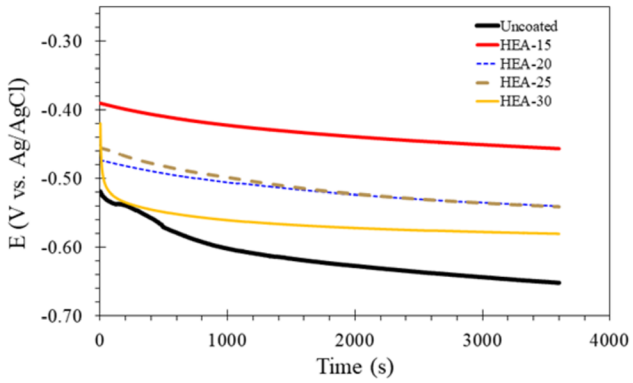

Fig. 6 Potential versus time curves of the uncoated and HEA-coated 1020 carbon steel in 3.5 wt.% NaCl solution at room temperature

in the Nyquist plots of the HEA-coated samples. The corrosion behavior of the 1020 carbon steel was, therefore, altered by the electrodeposited film. The EIS response was characterized by a capacitive loop that becomes more flattened as the deposition time increased from 15 to 30 min. It is well known from the literature that the diameter of the capacitive semicircle is related to the charge transfer resistance of the electrode surface which is an indication of its corrosion resistance (Ref 43). The HEA-15 sample exhibited the largest diameter of the capacitive loop, indicating its superior corrosion resistance when compared to the coatings obtained with longer deposition times. This result agrees well with the findings of the potential versus time curves (Fig. 6), pointing to a deleterious effect of the deposition time on the electrochemical stability of the CoCrFeNiAl coatings. Bode magnitude plots (Fig. 7b) confirm the superior corrosion resistance of the HEA-15 sample, as denoted by its high impedance modulus at 0.01 Hz. The phase angle plots (Fig. 7c) indicate that the uncoated substrate exhibits one single time constant, typical of carbon steels freely corroding in sodium chloride solutions, showing a completely resistive behavior with an evident drop-off of the phase angle values at the lowest frequencies (Ref 44). The CoCrFeNiAl coating shifted the phase angles to more capacitive values in the low frequency domain. The HEA-15 sample displayed a peak phase angle of − 55° at 4 mHz, while it reached more resistive values for all other HEA-coated samples.

Potentiodynamic polarization curves of the uncoated and HEA-coated carbon steel substrate after 1 h of immersion in 3.5 wt.% NaCl solution at room temperature are shown in Fig. 8. Relevant electrochemical parameters were determined from these curves, as displayed in Table 3. The corrosion potential (E_{corr}) and corrosion current density (i_{corr}) were obtained by the Tafel extrapolation method, considering only the cathodic branch. For the samples that exhibited a passive

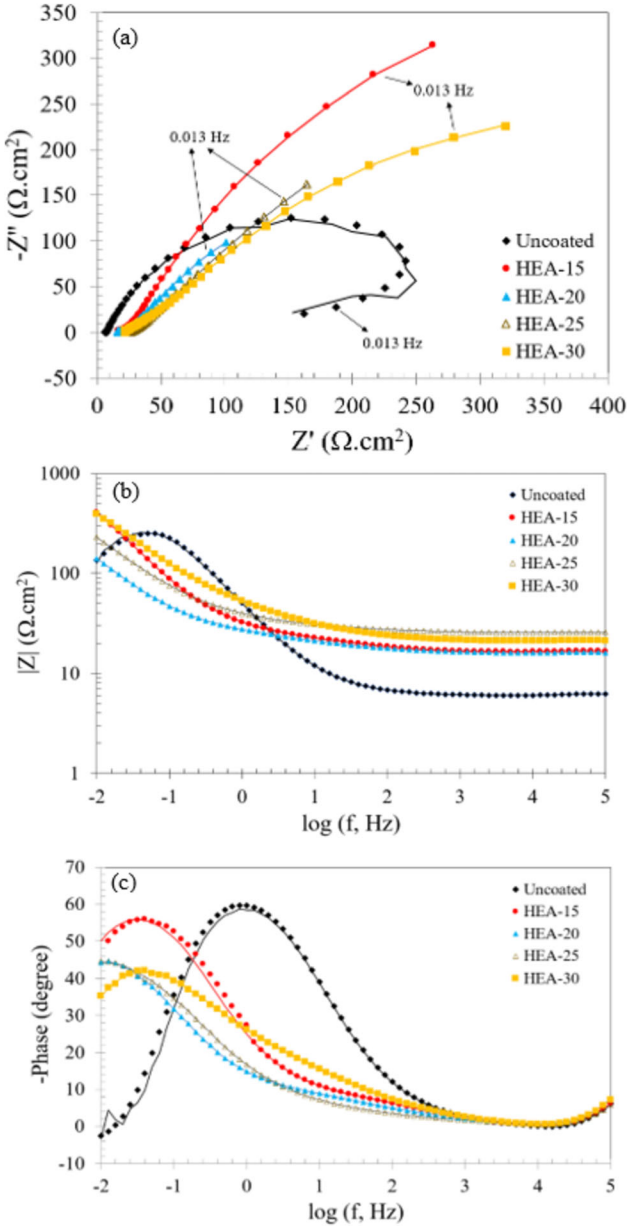

Fig. 7 EIS results of the uncoated and HEA-coated 1020 carbon steel samples after 1 h of immersion in 3.5 wt.% NaCl solution at room temperature: (a) Nyquist; (b) Bode magnitude plots; and (c) Bode phase angle plots

range in the polarization curve the values of passive current density (i_{pass}), breakdown potential (E_b) and passive range ($\Delta E = E_b - E_{corr}$) were also determined. The values of i_{pass} were taken at the middle of the passive range.

The uncoated substrate exhibited active corrosion behavior, indicating its susceptibility to corrosion in the sodium chloride solution in agreement with the EIS results (Fig. 7). The HEA coating changed the corrosion mechanism. All coated samples exhibited passivity. However, the stability of the passive film was dependent on the deposition time. For instance, the HEA-25 and HEA-30 samples showed incipient passivity, as denoted by their relatively low breakdown potentials and narrow passive ranges. Conversely, for lower deposition times, a different electrochemical response was seen. The breakdown potential and passive range increased for the HEA-20 sample.

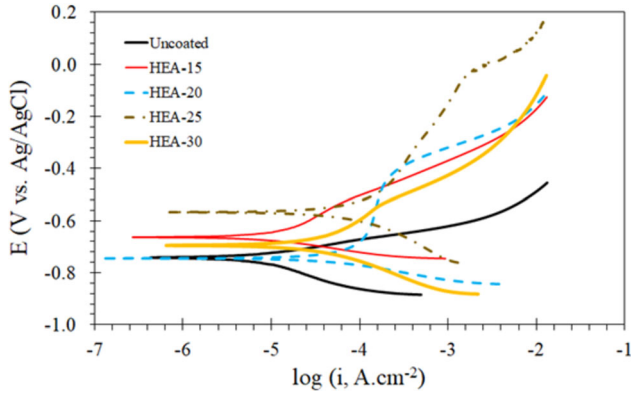

Fig. 8 Potentiodynamic polarization curves of the uncoated and HEA-coated carbon steel substrate after 1 h of immersion in 3.5 wt.% NaCl solution at room temperature

The maximum values of E_b and ΔE were obtained for the HEA-15 sample, indicating its superior corrosion resistance and passive film stability.

4. Discussion

The effect of the deposition time on the structure, morphology, surface composition, and corrosion behavior of CoCrFeNiAl coatings was revealed from the results shown in the previous section.

As shown in section 3.4, the deposition time influenced the corrosion resistance of the HEA-coated samples. The electrochemical activity was reduced by the presence of the CoCrFeNiAl coatings when compared to the bare carbon steel substrate. As the deposition time increased from 15 to 30 min, the open-circuit potential exhibited a descending trend (Fig. 6). The impedance modulus was higher for the HEA-15 sample (Fig. 7b), which also showed the widest passive range and the highest breakdown potential, as shown in Table 3. The detrimental effect of increasing the deposition time can be related either to morphological, structural, or compositional aspects.

The XRD patterns exhibited in Fig. 2 did not show significant effects of the deposition time on the phase structure of the deposited coatings.

The surface chemistry was investigated by XPS, and the results showed that a complex mixture of different oxidized species was found for all samples. The surface oxide film consisted of FeO, Fe_2O_3, Fe_3O_4, FeOOH, CoO, Co_3O_4, Cr_2O_3, $Cr(OH)_3$, NiO, $Ni(OH)_2$, Al_2O_3, and AlOOH. The deposition time did not alter the surface chemistry of the CoCrFeNiAl coatings.

The morphological features of high-entropy coatings play a crucial role in the corrosion protection ability of the deposited layer (Ref 45, 46). As shown in Sect. 3.2, the coating morphology was affected by the deposition time. The HEA-15 sample (Fig. 3a) exhibited the most compact surface. The coating thickness increased with the plating time, as expected for the electrodeposition (Ref 47). However, this was not accompanied by an enhancement of the corrosion resistance, as shown in section 3.4. The defective nature of the thicker CoCrFeNiAl coatings (Fig. 3b, c and d) was detrimental to the

Table 3 Electrochemical parameters determined from the potentiodynamic polarization curves shown in Fig. 7

Sample	E_{corr}, $mV_{Ag/AgCl}$	i_{pass}, $10^{-4}A.cm^{-2}$	E_b, $mV_{Ag/AgCl}$	ΔE, mV
Uncoated	− 704	…	…	…
HEA-15	− 567	4.47	− 28	539
HEA-20	− 745	1.38	− 431	314
HEA-25	− 664	0.32	− 533	131
HEA-30	− 695	0.81	− 549	146

corrosion resistance of the HEA-20, HEA-25, and HEA-30 samples.

In fact, coating morphology has been the subject of several investigations on the correlation between electrodeposition parameters and the corrosion resistance of the deposits (Ref 48, 49). Key issues are related to the porosity, hydrogen permeation, and metal ions release through the coating layer, depending on processing conditions during the electrodeposition (Ref 50-52). Li et al. (Ref 53) have shown that the compactness of electrodeposited FeCoCrNi medium-entropy alloy coating on Al substrate was dependent on the deposition temperature, thus influencing its corrosion resistance in 3.5 wt.% NaCl solution. Cheng et al. (Ref 54) observed that the porosity of FeCoCrNiMn-WC composite coatings obtained by electrodeposition on Cu substrates was dependent on the deposition parameters, especially the concentration of nanoparticles, giving rise to distinct corrosion resistances. Coating compactness is reported to play a central role in the corrosion resistance of electrodeposited layers (Ref 55).

From the above findings, the corrosion mechanism of the CoCrFeNiAl-coated carbon steel samples can be illustrated in Fig. 9. For the HEA-15 sample (Fig. 9a), the CoCrFeNiAl layer is thinner but less defective, favoring the corrosion protection ability in the sodium chloride solution. As the deposition time increased, a thicker and more defective coating layer was formed (Fig. 9b).

5. Conclusions

CoCrFeNiAl high-entropy alloy coatings were successfully electrodeposited on 1020 carbon steel substrate at different plating times (15, 20, 25, and 30 min). The effect of the deposition time on coating structure, morphology, composition, and corrosion behavior was assessed. The main findings can be described as follows:

(1) The coating structure was not affected by the deposition time, exhibiting one single BCC phase.
(2) As the deposition time increased from 15 to 30 min, the HEA layer became thicker, but more defective.
(3) The surface chemistry of all samples showed a complex mixture of cobalt, chromium, iron, nickel, and aluminum oxidized species which was not significantly affected by the deposition time.
(4) The corrosion resistance of the coated samples was dependent on the deposition time. The results showed that best corrosion protection ability was obtained at a deposition time of 15 min. Longer treatment times were detrimental to the corrosion resistance due to the defective morphology of the HEA coatings.

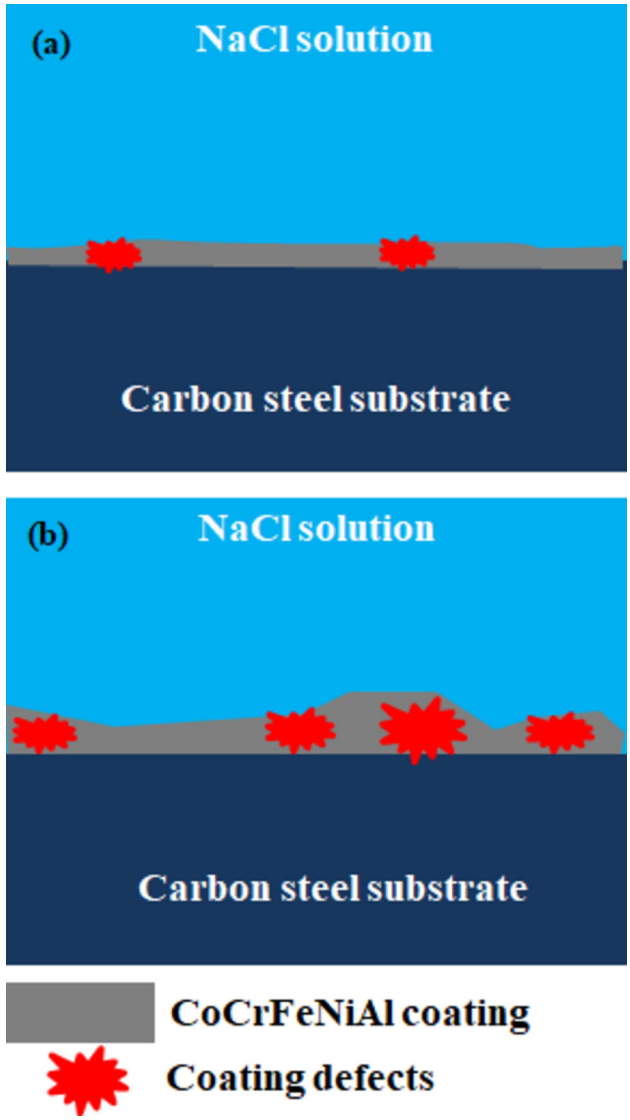

Fig. 9 Schematic representation of the effect of the deposition time on the corrosion resistance of the HEA-coated samples: (a) 15 min of treatment; (b) longer treatment times (20, 25, and 30 min)

Acknowledgments

The authors are grateful to the Brazilian National Council for Scientific and Technological Development (CNPq–Proc. 405420/2021-8) for the financial support. Fernanda Santos Fogassa is thankful to the CNPq for the research grant (102992/2023-1). The Central Multiuser Facilities (CEM) of UFABC is acknowledged for the experimental support. The authors would like to thank the Central de Análises Multiusuários do IPEN for the support.

Funding

The Article Processing Charge (APC) for the publication of this research was funded by the Coordenação de Aperfeiçoamento de Pessoal de Nível Superior - Brasil (CAPES) (ROR identifier: 00x0ma614).

References

1 L. Moravcikova-Gouvea, I. Moravcik, M. Omasta, J. Vesely, J. Cizek, P. Minárik, J. Cupera, A. Zádera, V. Jan, and I. Dlouhy, High-Strength $Al_{0.2}Co_{1.5}CrFeNi_{1.5}Ti$ High-Entropy Alloy Produced by Poder Metallurgy and Casting: A Comparison of Microstructures, Mechanical and Tribological Properties, *Mater Charact*, 2020, **159**, p 110046. https://doi.org/10.1016/j.matchar.2019.110046

2 L. Jiang, Y. Lu, Y. Dong, T. Wang, Z. Cao, and T. Li, Annealing Effects on the Microstructure and Properties of Bulk High-Entropy $CoCrFeNiTi_{0.5}$ Alloy Casting Ingot, *Intermetallics*, 2014, **44**, p 37–43. https://doi.org/10.1016/j.intermet.2013.08.016

3 P. Martin, C. Aguilar, and J.M. Cabrera, A Review on Mechanical Alloying and Spark Plasma Sintering of Refractory High-Entropy Alloys: Challenges, Microstructures, and Mechanical Behavior, *J. Mater. Res. Technol.*, 2024, **30**, p 1900–1928. https://doi.org/10.1016/j.jmrt.2024.03.205

4 A. Nassar, A. Mullis, R. Cochrane, Z. Aslam, S. Micklethwaite, and L. Cao, Rapid Solidification of AlCoCrFeNi2.1 High-Entropy Alloy, *J. Alloys Compd.*, 2022, **900**, p 163350. https://doi.org/10.1016/j.jallcom.2021.163350

5 Z.U. Arif, M.Y. Khalid, A.A. Rashid, E.U. Rehamn, and M. Atif, Laser Deposition of High-Entropy Alloys: A Comprehensive Review, *Opt. Laser Technol.*, 2022, **145**, p 107447. https://doi.org/10.1016/j.optlastec.2021.107447

6 A. Günen, T. Lindner, M.S. Karakas, E. Kanca, G. Töberling, S. Vogt, M.S. Gök, and T. Lampke, Effect of the Boriding Environment on the Wear Response of Laser-Clad AlCoCrFeNi High Entropy Alloy Coatings, *Surf. Coat. Technol.*, 2022, **447**, p 128830. https://doi.org/10.1016/j.surfcoat.2022.128830

7 A.K. Basak, A. Kurdi, N. Radhika, J. Arputharaj, C. Prakash, A. Pramanik, and S. Shankar, Compressive Mechanical Properties of Thermal Sprayed AlCoCrFeNi High Entropy Alloy Coating, *J. Alloys Compd.*, 2024, **1003**, p 175721. https://doi.org/10.1016/j.jallcom.2024.175721

8 X. Zeng, Z. Liu, G. Wu, X. Tong, Y. Xiong, X. Cheng, X. Wang, and T. Yamaguchi, Microstructure and High-Temperature Properties of Laser Cladded $AlCoCrFeNiTi_{0.5}$ High-Entropy Coating on Ti6Al4V Alloy, *Surf. Coat. Technol.*, 2021, **418**, p 127243. https://doi.org/10.1016/j.surfcoat.2021.127243

9 S. Wang, Y. Sun, W. Cheng, Y. Chen, and J. Gu, High Temperature Oxidation Behavior of CoCrFeNiMo0.2 High-Entropy Alloy Coatings Produced by Laser Cladding, *Mater. Today Commun.*, 2024, **39**, p 108639. https://doi.org/10.1016/j.mtcomm.2024.108639

10 N.G. Kipkirui, T.-T. Lin, R.S. Kiplangat, J.-W. Lee, and S.-H. Chen, HiPIMS and RF Magnetron Sputtered $Al_{0.5}CoCrFeNi_2Ti_{0.5}$ HEA Thin-Film Coatings: Synthesis and Characterization, *Surf. Coat. Technol.*, 2022, **449**, p 128988. https://doi.org/10.1016/j.surfcoat.2022.128988

11 G.F.N. Freitas, W.S. Gomes, J.P.I. Souza, C.N. Pinotti, E.C. Passamani, M.F. Montemor, and R. Della Noce, Direct Electrodeposition of CoFeNiMoW High Entropy Alloy Thin Films from Aqueous Medium, *Mater. Chem. Phys.*, 2023, **309**, p 128438. https://doi.org/10.1016/j.matchemphys.2023.128438

12 K.S.K.J. Reddy, L.P.P. Chokkakula, and S.R. Dey, Strategies to Engineer FeCoNiCuZn High Entropy Alloy Composition Through Aqueous Electrochemical Deposition, *Electrochim. Acta*, 2023, **453**, p 142350. https://doi.org/10.1016/j.electacta.2023.142350

13 A.M.J. Popescu, F. Branzoi, M. Burada, J.C. Moreno, J. Anastasescu, I. Anasiei, M.T. Olaru, and V. Constantin, CoCrFeMnNi High-Entropy Alloy Thin Films Electrodeposited on Aluminum Support, *Coatings*, 2023, **13**, p 980. https://doi.org/10.3390/coatings13060980

14 F. Yoosefan, A. Ashrafi, and S.M.M. Vaghefi, Microstructure and Corrosion Properties of Electrodeposited CoCrFeMnNi High Entropy Alloy Coatings, *Front. Mater.*, 2022, **9**, p 891011. https://doi.org/10.3389/fmats.2022.891011

15 Z. Gao, Z. Niu, Z. Gao, J. Li, G. Bai, L. Ke, Y. Yu, and C. Zhang, Microstructure and Wear Behavior of in-situ Synthesized TiC-Reinforced CoCrFeNi High Entropy alloy by laser cladding, *Appl. Surf. Sci.*, 2024, **670**, p 160720. https://doi.org/10.1016/j.apsusc.2024.160720

16 P.D. Babu, P. Dongre, A. Moganraj, A. Nambiraj N., G. Manivasagam, and J. Sure, Impact of Copper and Manganese on Phase Transformation, Microstructural Development and Material Strength in CoCrFeNi High-Entropy Alloys Through Mechanical Alloying, *Mater. Today Commun.*, 2024, **40**, p 109579. https://doi.org/10.1016/j.mtcomm.2024.109579

17 F. Prusa, A. Senkova, J. Kucera, J. Capek, and D. Vojtech, Properties of a High-Strength Ultrafine-Grained CoCrFeNiMn high-Entropy Alloy Prepared by Short-Term Mechanical Alloying and Spark Plasma Sintering, *Mater. Sci. Eng. A*, 2018, **734**, p 341–352. https://doi.org/10.1016/j.msea.2018.08.014

18 X. Zhang, Y. Yu, B. Ren, Z. Liu, T. Li, L. Wang, and Z. Qiao, Design of a Novel CoCrFeNiCu0.3 High Entropy Alloy with Desirable Mechanical, Corrosion and Anti-Bacterial Properties via Adjusting Cu Distribution, *Mater. Today Commun.*, 2023, **35**, p 105946. https://doi.org/10.1016/j.mtcomm.2023.105946

19 M. Zhang, X. Zhang, M. Niu, Z. Jiang, H. Chen, and Y. Sun, High-Temperature Tribological Behavior of CoCrFeNiV High-Entropy Alloys: A Parallel Comparison with CoCrFeNiMn High-Entropy Alloys, *Tribol. Int.*, 2022, **174**, p 107736. https://doi.org/10.1016/j.triboint.2022.107736

20 A.I. Thorhallsson, I. Csáki, L.E. Geambazu, F. Magnus, and S.N. Karlsdottir, Effect of Alloying Ratios and Cu-Addition on Corrosion Behaviour of CoCrFeNiMo High-Entropy Alloys in Superheated Steam Containing CO_2, H_2S and HCl, *Corros. Sci.*, 2021, **178**, p 109083. https://doi.org/10.1016/j.corsci.2020.109083

21 A.S. Rogachev, S.G. Vadchenko, D.Y. Kovalev, N.A. Kochetov, M. Zhukovskyi, T. Orlova, and A.S. Mukasyan, Long Term Stability of a High-Entropy CoCrFeNiTi Alloy Fabricated by Mechanical Alloying, *J. Alloys Compd.*, 2023, **931**, p 167470. https://doi.org/10.1016/j.jallcom.2022.167470

22 Z. Rong, C. Wang, Y. Wang, M. Dong, Y. You, J. Wang, H. Liu, J. Liu, Y. Wang, and Z. Zhu, Microstructure and Properties of FeCoNiCrX (X = Mn,Al) High-Entropy Alloy Coatings, *J. Alloys Compd.*, 2022, **921**, p 166061. https://doi.org/10.1016/j.jallcom.2022.166061

23 C.B. Nascimento, U. Donatus, C.T. Ríos, and R.A. Antunes, Passive Film Composition and Stability of CoCrFeNi and CoCrFeNiAl High Entropy Alloys in Chloride Solution, *Mater. Chem. Phys.*, 2021, **267**, p 124582. https://doi.org/10.1016/j.matchemphys.2021.124582

24 P. Lyu, Q. Gao, T. Peng, H. Yuan, Q. Guan, J. Cai, H. Liu, and X. Liu, Microstructure and Properties of CoCrFeNiAlx (x=0.1, 0.5, 1) High-Entropy Alloys Enhanced by Laser Surface Remelting, *Mater Charact*, 2022, **185**, p 111717. https://doi.org/10.1016/j.matchar.2021.111717

25 S. Singh and C. Srivastava, Effect of Carbon Nanotube Incorporation on the Evolution of Morphology, Phase and Compositional Homogeneity, Surface Oxide Chemistry and Corrosion Behaviour of Electrodeposited FeCuMnNiCo-Carbon Nanotube Composite Coatings, *Electrochim. Acta*, 2023, **439**, p 141639. https://doi.org/10.1016/j.electacta.2022.141639

26 M.J.R. Haché, J. Tam, U. Erb, and Y. Zou, Electrodeposited NiFeCo-(Mo,W) High-Entropy Alloys with Nanocrystalline and Amorphous

Structures, *J. Alloys Compd.*, 2023, **952**, p 170026. https://doi.org/10.1016/j.jallcom.2023.170026
27 W.-R. Wang, W.-L. Wang, S.-C. Wang, Y.-C. Tsai, C.-H. Lai, and J.-W. Yeh, Effects of Al Addition on the Microstructure and Mechanical Property of AlxCoCrFeNi High-Entropy Alloys, *Intermetallics*, 2012, **26**, p 44–51. https://doi.org/10.1016/j.intermet.2012.03.005
28 A. Aliyu and C. Srivastava, Phase Constitution, Surface Chemistry and Corrosion Behavior of Electrodeposited MnFeCoNiCu High Entropy Alloy-Graphene Oxide Composite Coatings, *Surf. Coat. Technol.*, 2022, **429**, p 127943. https://doi.org/10.1016/j.surfcoat.2021.127943
29 X.-L. Shang, Z.-J. Wang, Q.-F. Wu, J.-C. Wang, J.-J. Li, and J.K. Yu, Effect of Mo Addition on Corrosion Behavior of High-Entropy Alloys CoCrFeNiMoxin Aqueous Environments, *Acta Metall. Sin.*, 2019, **32**, p 41–51. https://doi.org/10.1007/s40195-018-0812-7
30 H.-D. Wang, J.-N. Liu, Z.-G. Xing, Z.-G. Ma, X.-F. Cui, G. Jin, and B.-S. Xu, Microstructure and Corrosion Behaviour of AlCoFeNiTiZr High-Entropy Alloy Films, *Surf. Eng.*, 2020, **36**, p 78–85. https://doi.org/10.1080/02670844.2019.1625127
31 C. Zhang, L. Huang, S. Li, K. Li, S. Lu, and J. Li, Improved Corrosion Resistance of Laser Melting Deposited CoCrFeNi Series High-Entropy Alloys by Al Addition, *Corros. Sci.*, 2023, **225**, p 111599. https://doi.org/10.1016/j.corsci.2023.111599
32 M. Wang, C. Liu, G.Y. Bai, H.Y. Liu, Y.B. Liu, D.X. Fan, Z.X. Wang, and G.B. Pang, Enhancement of Surface Quality and Corrosion Resistance in 321 Stainless Steel by Electrochemical Machining, *Vacuum*, 2025, **240**, p 114487. https://doi.org/10.1016/j.jmrt.2025.08.043
33 E.E. El-Katori, M.I. Nessim, M.A. Deyab, and K. Shalabi, Electrochemical, XPS and Theoretical Examination on the Corrosion Inhibition Efficacy of Stainless Steel via Novel Imidazolium Ionic Liquids in Acidic Solution, *J. Mol. Liq.*, 2021, **337**, p 116467. https://doi.org/10.1016/j.molliq.2021.116467
34 Z. Wang, Z. Feng, and L. Zhang, Effect of High Temperature on the Corrosion Behavior and Passive Film Composition of 316L Stainless Steel in High H_2S-Containing Environments, *Corros. Sci.*, 2020, **174**, p 108844. https://doi.org/10.1016/j.corsci.2020.108844
35 Y. Yang, J. Cheng, S. Liu, H. Wang, and P. Dong, Effect of $NaAlO_2$ Sealing on Corrosion Resistance of 2024 Aluminum Alloy Anodized Film, *Mater. Corros.*, 2019, **70**, p 120–127. https://doi.org/10.1002/maco.20180327
36 Y. Zuo, S. Wang, Y. Tang, and Y. Zhou, The Inhibition of Sodium Oleate for Pitting Corrosion of Aluminum Alloy 2024 in 0.1 mol L^{-1} NaCl Solution, *J. Braz. Chem. Soc.*, 2015, **26**, p 1656–1663. https://doi.org/10.5935/0103-5053.20150139
37 Z. Wang, K. Ma, L. Feng, J. Cui, and Y. Zhao, Corrosion Resistance of $FeCrMn_xAlCu$ High-Entropy Alloys in 0.5 M H_2SO_4 Solution, *Mater. Today Commun.*, 2024, **40**, p 109864. https://doi.org/10.1016/j.mtcomm.2024.109864
38 X. Yang and X. Li, Research on the Synergistic Damage Behavior of Tribocorrosion of CoCrFeNi-X (Ti, Mn, Mo, Al) High-Entropy Alloys, *Tribol. Int.*, 2025, **201**, p 100185. https://doi.org/10.1016/j.triboint.2024.110185
39 I. Voiculescu, S.J. Brito-Garcia, O.M. González-Díaz, and J. Mirza-Rosca, Mechanical Characteristics and Corrosion Behavior of Two New Titanium Alloys, *Metals*, 2023, **13**, p 1729. https://doi.org/10.3390/met13101729
40 Y.A.N. Maocheng, X.U. Jin, Y.U. Libao, W.U. Tangqing, S.U.N. Cheng, and K.E. Wei, EIS Analysis on Stress Corrosion Initiation of Pipeline Steel Under Disbanded Coating in Near-Neutral pH Simulated Soil Electrolyte, *Corros. Sci.*, 2016, **110**, p 23–34. https://doi.org/10.1016/j.corsci.2016.04.006
41 Z. Dong, B. Ter-Ovanessian, H. Abe, N. Mary, Y. Watanabe, and B. Normand, Design of an EIS-Based Sensor for Indirect Non-invasive Corrosion Inspection, *Corros. Sci.*, 2025, **254**, p 113029. https://doi.org/10.1016/j.corsci.2025.113029
42 Y.C.S. Moyeme, S. Betelu, J. Bertrand, K.G. Serrano, and I. Ignatiadis, Corrosion Behavior of X65 API 5L Carbon Steel Under Simulated Storage Conditions: Influence of Gas Mixtures, Redox States, and Temperature Assessed Using Electrochemical Methods for up to 100 Hours, *Metals*, 2025, **15**, p 221. https://doi.org/10.3390/met15020221
43 M. Ragab and M.A. Bedair, The Effect of Permanent Magnet Stirring on the Corrosion Resistance of Sn-2.0Ag-0.5Cu-2Zn Solder Alloys in NaCl Solution, *Mater. Chem. Phys.*, 2023, **302**, p 127774. https://doi.org/10.1016/j.matchemphys.2023.127774
44 M.P. Garcia, G.L. Mantovani, R.V. Kumar, and R.A. Antunes, Corrosion Behavior of Metal Active Gas Welded Joints of a High-Strength Steel for Automotive Application, *J. Mater. Eng. Perform.*, 2017, **26**, p 4718–4731. https://doi.org/10.1007/s11665-017-2900-7
45 M. Mohan, U. Pandel, and K. Kumar, Phase Composition, Surface Chemistry and Electrochemical Studies of Electrodeposited AlMnFeCuNi High Entropy Alloy Composite Coatings Incorporated with Carbon Nanotubes, *Mater. Res. Express*, 2024, **11**, p 046643. https://doi.org/10.1088/2053-1591/ad2a88
46 Y. Wang, X. Han, M. Zhang, X. Duan, R. Guo, B. Niu, H. Wang, X. Gao, and H. Yan, Microstructure and Corrosion Resistance of FeCrCoNiAl Coatings on Stainless Steel: Role of Deposition Solution, Parameters, and Aluminum Concentration, *J. Alloys Compd.*, 2025, **1040**, p 183446. https://doi.org/10.1016/j.allcom.2025.183446
47 A. Shah, B. Chauhan, R.K. Rai, and B.M. Mundotiya, Electrodeposition of high entropy alloy coating: A brief of the deposition parameters, futuristic trends in chemical, *Material Sciences and Nano Technology*, 2024, IIP Series, Volume 3, Book 12, Part 1, Chapter 5
48 H. Li, H. Wang, K. Tang, L. Liu, M. Yan, W. Jian, H. Wang, and L. Ren, Preparation of WS_2-Modulated Ni-W-P Superhydrophobic Coatings via One-Step Electrodeposition–Microstructure Optimization, Corrosion Resistance Enhancement, and Multifunctional Performance Improvement, *Colloids Surf A Physicochem Eng Asp*, 2025, **725**, p 137729. https://doi.org/10.1016/j.colsurfa.2025.137729
49 S.R. Torabianfard, R. Jamaati, and H.J. Aval, Investigation of the Influence of Deposition Time on Morphology, Crystallographic Texture, and Corrosion Resistance of ZnO Coatings on Titanium Substrates, *Surf. Coat. Technol.*, 2025, **511**, p 132309. https://doi.org/10.1016/j.surfcoat.2025.132309
50 A.T. Cabral, A.R.G. Oliveira, G.Y. Koga, L.C. Rigoli, C.L.F. Rocha, and C.A.C. Souza, Electrodeposited Zinc Cellulose Nanocrystals Composite Coatings: Morphology, Structure, Corrosion Resistance and Electrodeposition Process, *J. Mater. Res. Technol.*, 2024, **33**, p 1569–1580. https://doi.org/10.1016/jmrt.2024.09.153
51 D.T.M. Thanh, P.T. Nam, N.T. Phuong, L.X. Que, N.V. Anh, T. Hoang, and T.D. Lam, Controlling the Electrodeposition, Morphology and Structure of Hydroxyapatite Coating on 316L Stainless Steel, *Mater. Sci. Eng. C*, 2013, **33**, p 2037–2045. https://doi.org/10.1016/j.msec.2013.01.018
52 F. Bakhtiarifard and N. Nayebpashaee, Effect of SiC Nanoparticles on the Wear and Corrosion Resistance of Ag-Si Composite Coatings Prepared by Electrodeposition Technique, *Appl. Surf. Sci. Adv.*, 2025, **28**, p 100791. https://doi.org/10.1016/j.apsadv.2025.100791
53 J. Li, Y. Ma, Z. Li, J. Zhang, and J. Zhang, Effect of Electrodeposition Parameters on the Morphology and Corrosion Resistance of a FeCoNiCr Medium-Entropy Alloy Coating on a Conductive Al Alloy Surface, *Mater. Today Commun.*, 2025, **49**, p 114367. https://doi.org/10.1016/j.mtcomm.2025.114367
54 Y. Cheng, C. Wang, M. Dong, Y. You, W. Cheng, W. Xie, Z. Wang, L. Wang, X. Zhang, and Y. Wang, Performance of FeCoNiCrMn-WC High-Entropy Alloy Coatings Fabricated by Composite Electrodeposition, *Intermetallics*, 2025, **187**, p 109003. https://doi.org/10.1016/j.intermet.2025.109003
55 S.R. Torbianfard, B. Jamaati, and H.J. Aval, Revealing the Morphology, Crystallographic Texture, and Corrosion Resistance of Electrodeposited ZnO Coatings on Pure Titanium Surfaces, *JOM*, 2025, **77**, p 5585–5599. https://doi.org/10.1007/s11837-025-07406-y